Integrative genome analysis of somatic p53 mutant osteosarcomas identifies Ets2-dependent regulation of small nucleolar RNAs by mutant p53 protein

Rasoul Pourebrahim,[1] Yun Zhang,[1] Bin Liu,[1] Ruli Gao,[1] Shunbin Xiong,[1] Patrick P. Lin,[2] Mark J. McArthur,[3] Michael C. Ostrowski,[4] and Guillermina Lozano[1]

[1]Department of Genetics, University of Texas MD Anderson Cancer Center, Houston, Texas 77030, USA; [2]Department of Orthopedic Oncology, University of Texas MD Anderson Cancer Center, Houston, Texas 77030, USA; [3]Department of Veterinary Medicine and Surgery, University of Texas MD Anderson Cancer Center, Houston, Texas 77030, USA; [4]Department of Cancer Biology and Genetics, The Ohio State University, Columbus, Ohio 43210, USA

***TP53* is the most frequently mutated gene in human cancer. Many mutant p53 proteins exert oncogenic gain-of-function (GOF) properties that contribute to metastasis, but the mechanisms mediating these functions remain poorly defined in vivo. To elucidate how mutant p53 GOF drives metastasis, we developed a traceable somatic osteosarcoma mouse model that is initiated with either a single *p53* mutation (p53R172H) or *p53* loss in osteoblasts. Our study confirmed that *p53* mutant mice developed osteosarcomas with increased metastasis as compared with *p53*-null mice. Comprehensive transcriptome RNA sequencing (RNA-seq) analysis of 16 tumors identified a cluster of small nucleolar RNAs (snoRNAs) that are highly up-regulated in p53 mutant tumors. Regulatory element analysis of these deregulated snoRNA genes identified strong enrichment of a common Ets2 transcription factor-binding site. Homozygous deletion of *Ets2* in p53 mutant mice resulted in strong down-regulation of snoRNAs and reversed the prometastatic phenotype of mutant p53 but had no effect on osteosarcoma development, which remained 100% penetrant. In summary, our studies identify Ets2 inhibition as a potential therapeutic vulnerability in p53 mutant osteosarcomas.**

[*Keywords*: p53; osteosarcoma; snoRNA; metastasis; Ets2]

Supplemental material is available for this article.

Received July 18, 2017; revised version accepted September 11, 2017.

Somatic missense mutation of *p53* is the most common *TP53* alteration observed in human cancers (Muller and Vousden 2014). The majority of these mutations is in the DNA-binding domain, resulting in loss of protein function (Olivier et al. 2010; Leroy et al. 2013). In addition, many *p53* mutants have gain-of-function (GOF) activities that are independent of loss of p53 function or their dominant-negative effect on wild-type p53 (Oren and Rotter 2010). Mice expressing germline *p53* mutations display more metastatic tumors when compared with *p53*-deficient mice (Lang et al. 2004; Olive et al. 2004). At the molecular level, several transcription factors, such as p63, p73, SREBP, NF-Y, VDR, and ETS2, have been identified to bind mutant p53 and drive gene expression, resulting in increased cell proliferation, modified cell membranes, increased cell invasion, enhanced cell survival, and metastasis (Muller et al. 2009; Do et al. 2012; Freed-Pastor et al. 2012; Kalo et al. 2012; Xiong et al. 2014; Kim and Lozano 2017). Importantly, interaction of mutant p53 with the Ets2 transcription factor was found recently to regulate chromatin modification and thereby modulate transcription on a whole-genome level (Do et al. 2012; Zhu et al. 2015). While mutant p53 controls a large number of genes, and several studies have identified mutant p53 target genes in cell lines, a comprehensive in vivo study has not been performed.

Tumor metastasis is the main cause of cancer-related deaths (Mehlen and Puisieux 2006). Metastatic cells acquire certain phenotypic plasticity that allows them to invade into the blood, survive an anchorage-independent environment, and home in to distant organs (Chaffer and Weinberg 2011). Increased tumor aggressiveness and

Corresponding author: gglozano@mdanderson.org
Article published online ahead of print. Article and publication date are online at http://www.genesdev.org/cgi/doi/10.1101/gad.304972.117.

higher metastatic potential are hallmarks of mutant p53 GOF in mouse models. Both germline mutant and Cre-Lox-STOP-lox conditional alleles of mutant p53 (LSL-mutp53) develop tumors that display a metastatic phenotype (Lang et al. 2004; Olive et al. 2004; Doyle et al. 2010; Morton et al. 2010; Muller and Vousden 2014). However, most of these studies have not been able to interrogate the potential role of mutant p53 in the modulation of the tumor microenvironment, mainly due to the fact that both germline and *LSL-mutantp53* mouse models harbor a p53 alteration in the stromal compartment that is known to have a deleterious impact on the tumor microenvironment (Patocs et al. 2007). In addition, precise evaluation of tumor cell migration and metastasis in p53 mutant mouse models has not been performed.

Recent studies have emphasized the important role of noncoding transcripts in normal and cancer cells (Djebali et al. 2012; Williams and Farzaneh 2012). Small nucleolar RNAs (snoRNAs) are a well-characterized class of noncoding transcripts 60–300 nucleotides (nt) in length that are encoded by ~500 different loci in the human genome (Kiss-Laszlo et al. 1996; Makarova and Kramerov 2011). They traditionally were considered to function as guide RNAs for the post-transcriptional modification of ribosomal RNAs (rRNAs). However, recent studies have discovered that exosomal snoRNAs released by tumors can bind Toll-like receptor3 (TLR3) and initiate an inflammatory cascade that promotes metastasis (Fabbri et al. 2012; Liu et al. 2016). There is a very limited understanding of expression of snoRNAs in cancer, and no major regulator of snoRNAs has been identified.

Here we describe a traceable somatic mouse model using a new conditional mutant *p53* allele combined with fluorescent labeling targeted to osteoblasts. Through our ability to image micrometastasis, we show that mutant *p53* tumors display increased metastasis compared with *p53*-null osteosarcomas. Moreover, we demonstrate that mutant p53 drives the expression of a cluster of snoRNAs through the Ets2 transcription factor. We further show that ablation of *Ets2* down-regulates these snoRNA genes and abrogates the prometastatic phenotype of mutant p53. To our knowledge, this is the first report showing regulation of snoRNA genes in cancer by mutant p53 and the Ets2 transcription factor. Our findings expand our understanding of the role of mutant p53 in metastasis, which may have broad translational significance in the diagnosis and treatment of tumors with mutant p53.

Results

A traceable osteosarcoma model driven by conditional mutant p53

We sought to generate a robust traceable mutant p53-dependent cancer model that would allow us to trace tumor cells and precisely identify micrometastases. We chose to use the osteosarcoma model because (1) it is known that loss or mutation of *p53* is sufficient to generate osteosarcomas, and (2) metastasis to the lung is common in osteosarcomas (Bielack et al. 2002). We made use of a new mutant *p53* allele, $p53^{wm\text{-}R172H}$ (abbreviated here as $p53^{wm172}$), as described (Y Zhang, S Xiong, B Liu, V Pant, F Celii, G Chau, AC Elizondo-Fraire, P Yang, MJ You, AK El-Naggar, et al., in prep.). This allele normally expresses wild-type p53 but, upon Cre-mediated recombination, expresses the p53R172H missense mutation. In this model, the tumor stroma and immune system remain wild type for p53, and therefore the premetastatic niche at the site of metastasis is not influenced by p53 haploinsufficiency as in other models.

The targeting strategy for the $p53^{wm172}$ allele was designed to maintain normal p53 expression from the endogenous locus prior to Cre-mediated recombination (Fig. 1A). Briefly, a partial wild-type *p53* cDNA encoding exons 5–11 (including the poly A signal), flanked by loxP sites, was inserted into intron 4 of the mutant *p53R172H* allele. The resulting allele expresses wild-type p53 at physiologic levels driven by the endogenous *Trp53* promoter (Y Zhang, S Xiong, B Liu, V Pant, F Celii, G Chau, AC Elizondo-Fraire, P Yang, MJ You, AK El-Naggar, et al., in prep.). Upon Cre-mediated recombination, the inserted cDNA sequence is removed, and the mutant *p53* locus is identical to the germline *p53R172H* allele that was generated previously in our laboratory (Lang et al. 2004).

To express mutant p53R172H specifically in the osteoblast lineage, we used the *Osx-Cre::GFP* mouse (*Osx-Cre*) that harbors a bacterial artificial chromosome (BAC), which includes the tetracycline transactivator (tTA) sequence driving the GFP/Cre fusion protein under the control of the Osterix (*Sp7*) promoter (Fig. 1B; Rodda and McMahon 2006). The specificity of *Osx-Cre* to osteoblasts (and not other mesenchymal lineages) was verified previously by others (Rodda and McMahon 2006; Berman et al. 2008). Since the expression of GFP from the *Osx-Cre::GFP* transgene is limited to the preosteoblast lineage and is lost upon cell differentiation/transformation (Mizoguchi et al. 2014), we used the $Rosa^{mTmG}$ (*mTmG*) reporter allele that expresses membrane-localized red fluorescence in general and green fluorescence in *Cre*-recombinase-expressing cells (Fig. 1B). In order to evaluate how well the *mTmG* allele worked, we examined *Osx-Cre;mTmG* mice and analyzed GFP expression in sections of long bones at 3 mo of age. In a cross-section of the bone, the expression of GFP (Fig. 1B, green) was present exclusively in the trabecular osteoblasts and osteocytes, while the bone stromal cells and hematopoietic lineages expressed tdTomato (Fig. 1B).

To delete p53 in the osteoblasts, we used a $p53^{fl}$ allele that has a LoxP site in introns 2 and 11 (Jonkers et al. 2001). Upon expression of Cre-recombinase, exons 2–10 are deleted, resulting in a null allele. To evaluate the functionality of $p53^{wm172}$ and $p53^{fl}$ alleles before and after recombination, we isolated bones from *Osx-Cre;mTmG*, *Osx-Cre;mTmG;*$p53^{wm172/+}$, *Osx-Cre;mTmG;*$p53^{wm172/fl}$, and *Osx-Cre;mTmG;*$p53^{fl/fl}$ mice (three each) and, after mechanical and enzymatic cell dissociation, separated them by FACS-based sorting into GFP^+ cells (osteoblasts) and $tdTomato^+$ (mesenchymal stroma and hematopoietic) cells (Fig. 1C,D). The population of osteoblasts (GFP^+) was increased in *Osx-Cre;mTmG;*$p53^{wm172/fl}$ mice (26.6% ±

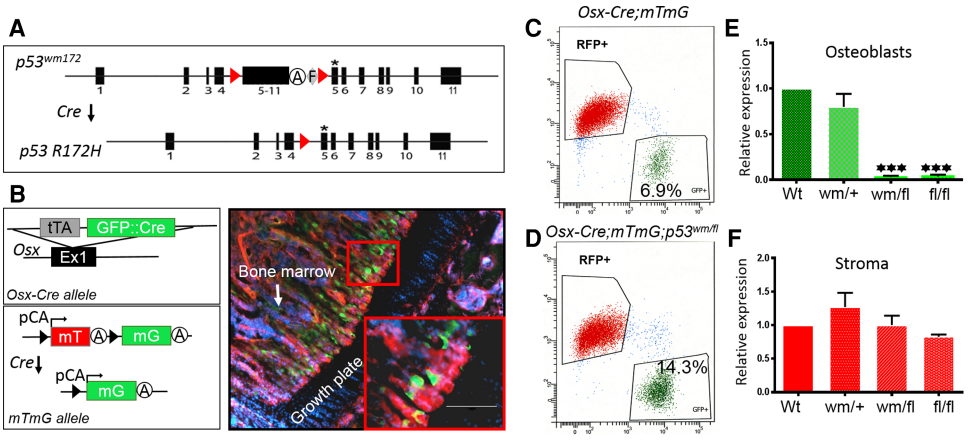

Figure 1. Generation of a traceable conditional mutant p53 osteosarcoma model. (*A*) Schematic representation of the conditional mutant *p53* allele ($p53^{wm172}$). Upon *Cre*-mediated recombination, the wild-type cDNA encompassing the indicated exons is deleted, resulting in expression of mutant p53R172H. (A) Polyadenylation; (F) FRT site. (*B*) Schematic representation of the *Osx-Cre* and *mTmG* alleles. *Cre* expression is regulated by the endogenous *Ostrix* promoter. Recombination of *mTmG* switches the fluorescence from red (tdTomato) to green (GFP). Direct fluorescence image of a longitudinal tibia section from a 3-mo-old *Osx;Cre;mTmG* mouse showing the osteoblasts (green) surrounded by red stromal cells. All cells were marked with DAPI (blue). (*C*,*D*) A representative FACS analysis of isolated cells derived from *Osx;Cre;mTmG* and *Osx;Cre;mTmG; p53*$^{wm172/fl}$ showing the population of osteoblasts (green) and stromal cells. Relative expression levels of *p21* mRNA normalized to expression of *Hprt* mRNA as a reference gene in isolated osteoblasts (*E*) and corresponding stroma (*F*). Statistical significance is marked with stars. (***) $P < 0.001$ by *t*-test. (tTA) Tetracycline-controlled transcriptional activation; (pCA) chicken β-actin promoter.

10%) in comparison with *Osx-Cre;mTmG* mice (8.3% ± 1%), suggesting that p53 mutation in osteoblasts has a proproliferative effect on osteoblasts, as described previously (Lengner et al. 2006). In order to evaluate p53 activity after recombination of $p53^{wm172}$ and $p53^{fl}$ alleles in the osteoblasts, we isolated the osteoblasts from bones and analyzed the expression of *p21*, an established p53 target gene, in sorted cells derived from bones isolated from mice (Fig. 1E,F). The expression of *p21* was significantly down-regulated in the osteoblasts (GFP$^+$) derived from *Osx-Cre;mTmG;*$p53^{wm172/fl}$ and *Osx-Cre;mTmG;*$p53^{fl/fl}$ mice (Fig. 1E), whereas its expression in the stromal cells from the same tissue (tdTomato$^+$) remained comparable with p53 wild type (Fig. 1F), suggesting that the p53 function is lost only in GFP$^+$ cells. Together, these data further confirm the fidelity of *mTmG* and $p53^{wm172}$ alleles and the functionality of the *Osx-Cre* transgene.

p53 *mutation in osteoblasts results in metastatic osteosarcoma*

In order to study the role of mutant p53 in metastatic osteosarcoma, we established three cohorts of mice: *Osx-Cre;mTmG;*$p53^{fl/fl}$ ($n = 43$), *Osx-Cre;mTmG;*$p53^{wm172/fl}$ ($n = 29$), and *Osx-Cre;mTmG;*$p53^{wm172/+}$ ($n = 20$). All cohorts developed osteosarcoma with complete penetrance mainly in the long bones, including the distal femur, proximal tibia, and humerus, as well as the pelvis, jaw, spine, and skull (Supplemental Fig. S1). Osteosarcoma of the jaw was twice as frequent in *Osx-Cre;mTmG;*$p53^{fl/fl}$ as in *Osx-Cre;mTmG;*$p53^{wm172/fl}$ mice (Supplemental Fig. S1). We also found primary osteosarcomas in the livers and spleens of two mice without any other primary tumors, indicative of extraskeletal osteosarcomas (Supplemental Fig. S2). The histologic diagnosis of extraskeletal osteosarcoma is based on the observation of the osteoid matrix and bone formation in a sarcomatous cellular background, as specific markers are not available. MicroCT of osteosarcomas revealed a mixed lytic and blastic lesion with cortical bone destruction reminiscent of human osteoblastic osteosarcoma (Fig. 2A,B). Histopathology of tumors confirmed the presence of osteoid-forming tumor cells that were mostly poorly differentiated or anaplastic (Fig. 2C), with areas of calcified bone matrix, as demonstrated by Alizarin Red staining (Supplemental Fig. S3A,B). Tumors derived from *Osx-Cre,* $p53^{wm172/fl}$ mice were strongly positive for p53 staining, as evaluated by immunohistochemistry (Supplemental Fig. S3C). Necropsy examination revealed macroscopic metastatic tumors in some mice (Fig. 2D,E), but, in most of cases, multiple serial lung sections were necessary to detect micrometastasis. In addition to tumor development, dental malocclusion was noted in mice with the *Osx-Cre* allele, and teeth had to be trimmed.

In order to evaluate tumor migration and metastasis, we developed a tracing strategy to visualize malignant cells by multicolor immunofluorescence imaging. Tumor cells were readily detected by their bright-green fluorescence surrounded by nonmalignant tissue, such as muscle and bone marrow (Fig. 2F). We were also able to accurately visualize metastasis at both the macroscopic (Fig. 2G) and microscopic levels (Fig. 2H) in the lungs as the main site of metastasis as well as the liver (Fig. 2I,J).

Kaplan-Meier analysis of survival showed significantly better survival for *Osx-Cre,*$p53^{wm172/fl}$ mice (median survival 354 d) compared with *Osx-Cre,*$p53^{fl/fl}$ mice (median

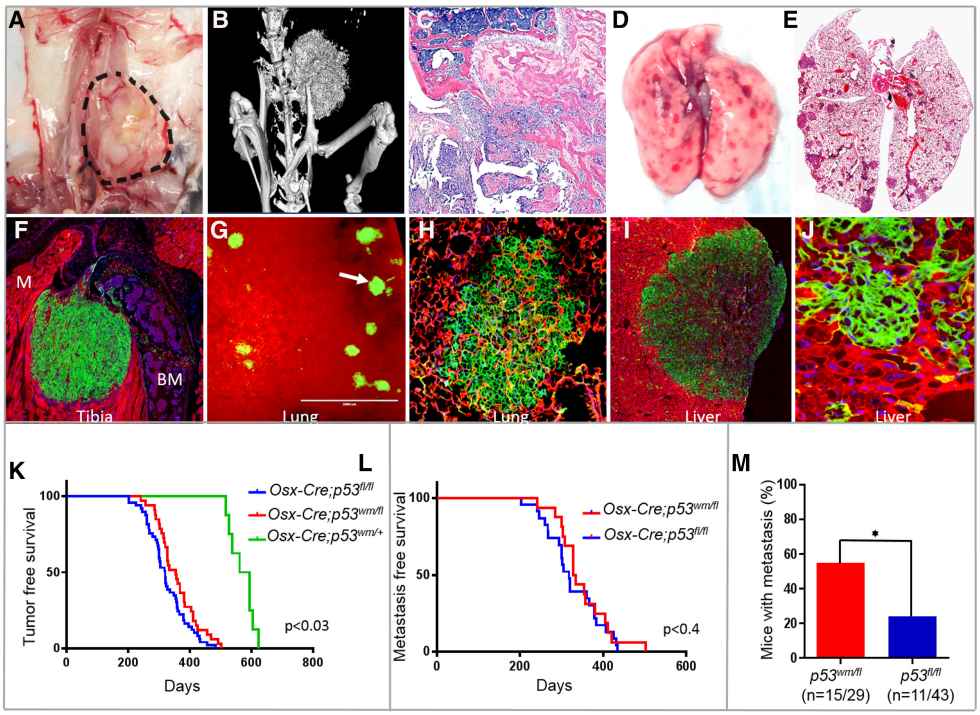

Figure 2. Characterization of tumor phenotype, survival, and metastasis. (*A*) Necropsy image of an osteosarcoma of the pelvis showing a retroperitoneal whitish mass. (*B*) MicroCT scan of the tumor in *A* showing a mass extending from the iliac crest with scattered calcifications. (*C*) Histopathology of a p53 mutant osteosarcoma stained with hematoxylin and eosin (H&E) showing a poorly differentiated osteosarcoma with osteoid formation and a high mitotic index arising from the growth plate of the tibia. (*D*) Representative image of metastatic osteosarcoma nodules in the lungs. (*E*) H&E-stained section of the lungs from *D*. (*F*) Direct fluorescent image of an early stage osteosarcoma in a p53 mutant mouse derived from a growth plate showing tumor cells (green) invading into the muscle (M) and bone marrow. (*G*) A macroscopic view of direct immunofluorescence of a multifocal lung metastasis showing malignant cells (green) embedded into alveoli. (*H*) Microscopic view of a lung metastasis showing tumor cells (green) surrounded by normal lung tissue. (*I*) Direct fluorescent image of a metastatic nodule in the liver. (*J*) High-magnification image of *I*. (*K*) Kaplan-Meier plot of tumor-free survival in conditional p53 mutant and p53-null mice. (*L*) Kaplan-Meier plot of metastasis-free survival in conditional p53 mutant and p53-null mice. (*M*) A bar chart representing the number of mice with the indicated genotypes that developed metastatic osteosarcomas (percentage). (*) $P < 0.05$ by *t*-test.

survival 320 d; $P < 0.03$) (Fig. 2K). The survival advantage was due to a later onset of tumor development, as there was no difference in the slope of the lines between the two groups. As expected, *Osx-Cre,p53*$^{wm172/+}$ mice had longer overall survival, with a median survival of 574 d. Analysis of metastasis-free survival did not show significant differences between p53 mutant and p53-null groups (Fig. 2L). These data suggest that despite having a later onset of tumor formation, *Osx-Cre,p53*$^{wm172/fl}$ mice had a more rapid onset of metastasis.

In order to evaluate metastatic behavior of osteosarcomas, we undertook a detailed processing of isolated lungs from mice after necropsy. For each lung, 12 sagittal serial sections of 100 µm were cut and fully examined for micrometastasis. We also used fluorescence microscopy to locate the pulmonary micrometastasis at single-cell resolution. We found that 15 of 29 (52%) mice with p53 mutant tumors (*Osx-Cre;p53*$^{wm172/fl}$) displayed metastasis in comparison with 11 of 43 (25%) mice with *p53*-null tumors (*Osx-Cre;p53*$^{fl/f}$; $P < 0.05$) (Fig. 2M). Analysis of metastatic nodules in the lungs revealed spots of calcified bone matrix, as judged by Alizarin Red staining (Supplemental Fig. S3B), suggesting that metastatic cells keep their osteogenic properties after seeding in the lungs. Taken together, the data indicate a prometastatic GOF role of mutant p53 and demonstrate the robustness of the model to identify micrometastases with high fidelity.

Mutant p53 GOF strongly up-regulates a set of snoRNAs

Mutant p53 proteins are known to have a broad effect on gene expression (Muller and Vousden 2014; Zhu et al. 2015). We therefore asked whether mutant p53 produces a specific gene signature that might explain the prometastatic GOF properties of mutant p53. We compared transcriptomes of eight primary osteosarcomas (four metastasizing and four nonmetastasizing) from *Osx-Cre; p53*$^{wm172/fl}$ mice with eight tumors (four metastasizing and four nonmetastasizing) derived from *Osx-Cre;p53*$^{fl/fl}$ mice. To minimize the effect of tumor heterogeneity and eliminate sampling bias, we extracted RNA and DNA from the same tissue for RNA sequencing (RNA-seq) and exome sequencing, respectively. We also set up

the RNA isolation and RNA-seq experiment to capture short transcripts. After quality and coverage filtering, the RNA-seq experiment yielded a mean of 23,529,331 mapped reads for each osteosarcoma sample. After mapping the sequencing reads to the mouse genome (mm10) using TopHat2, we first validated that all samples derived from p53 mutant tumors exhibited a single point mutation at amino acid 172 (Supplemental Fig. S4), as expected by reviewing the detected RNA-seq reads that were mapped to the *p53* gene. Differential gene expression analysis identified 434 genes that were differentially expressed (twofold change; false discovery rate [FDR]-adjusted $P < 0.05$) between p53 mutant versus p53-null tumors regardless of metastases (Fig. 3A,B). In addition, *p53* gene expression was significantly lower in all *p53*-null tumors ($P < 0.001$) (Fig. 3C). Strikingly, we found a cluster of 24 snoRNAs that were among the top 35 genes overexpressed in p53R172H as compared with *p53*-null tumors regardless of metastatic phenotype (Fig. 3D). The expression of the identified cluster of snoRNAs was highly up-regulated in all eight p53R172H osteosarcomas, whereas it was barely detectable in *p53*-null tumors (Fig. 3E). Since the majority of the snoRNAs resides in the intronic regions of host genes, we asked whether they were coregulated by the same promotors. Analysis of sequencing reads of RNAs that were expressed using Integrated Genome Viewer (IGV) indicated that the expression of the identified snoRNAs is independent of the expression of host genes, suggesting that they were controlled by different regulatory elements (Supplemental Fig. S5).

In addition to the snoRNA signature, p53 mutant tumors also demonstrated a distinct gene expression profile comprised of 409 genes that were differentially expressed between p53 mutant versus p53-null osteosarcomas. In order to evaluate the functional genetic network of p53 mutant-associated genes, we performed gene ontology (GO) analysis. We found several pathways associated with chromatin modifications, including histone deacetylases and methylases (Supplemental Fig. S6), suggesting that mutant p53 GOF is associated with epigenetic transcription regulatory elements as described by others (Pfister et al. 2015; Zhu et al. 2015). Of note, the snoRNA signature was not included in the GO analysis due to a lack of annotation of mouse snoRNAs.

Genetic deletion of the Ets2 transcription factor abrogates the mutant p53 prometastatic phenotype

Next, we sought to understand the mechanism by which mutant p53 up-regulates the expression of snoRNAs. Since mutant p53 binds other DNA-binding transcription factors and modulates their ability to regulate genes, we searched for potential regulatory elements of known transcription factors using MotifMap. This platform provides a genome-wide map of >380 known regulatory motifs and is powered to assess the accuracy of identified elements (Xie et al. 2009). We found that the Ets2-binding motif was highly enriched in eight of the 24 snoRNAs identified (Table 1). Since the intronically encoded snoRNAs are highly conserved between mice and humans (Tycowski et al. 1996), we used an available human ChIP-seq (chromatin immunoprecipitation [ChIP] combined with high-throughput sequencing) data set (downloaded from ENCODE) and analyzed the ETS2 occupancy of human

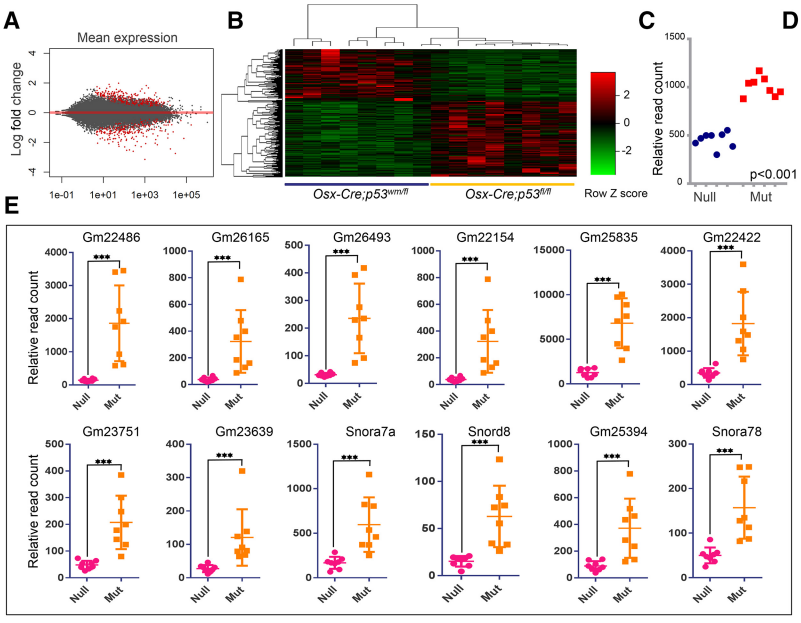

	Read	Log2 fold	*p*-value	Gene (Mouse)	Gene type	Orthologue (Human)
1	1001	3.1	2.33E-24	**Gm22486**	SnoRNA	SNORD94
2	273	2.6	1.14E-16	**Gm26165**	SnoRNA	SNORA70
3	133	2.5	2.80E-18	**Gm26493**	SnoRNA	SNORA46
4	181	2.5	9.14E-14	**Gm22154**	SnoRNA	SNORA55
5	16870	2.4	2.02E-09	**Gm23935**	miRNA	NA
6	107	2.3	6.19E-14	**Gm26316**	SnRNA	NA
7	666	2.3	3.03E-11	**Gm24187**	miRNA	NA
8	57	2.3	2.46E-12	**Gm23734**	SnoRNA	NA
9	353	2.2	6.46E-11	**Mir1949**	miRNA	NA
10	4039	2.1	3.41E-15	**Gm25835**	SnoRNA	SNORD10
11	1088	2.1	7.98E-13	**Gm22422**	SnoRNA	SNORD70E
12	3173	2.0	3.40E-12	**Rny3**	misc RNA	Y_RNA
13	28	2.0	2.27E-09	**Gm23346**	SnoRNA	SNORA5
14	423	1.9	4.10E-14	**Gm15662**	psudogene	pseudogene
15	69	1.9	1.13E-07	**Gm22620**	SnoRNA	SNORA1
16	128	1.9	1.74E-11	**Gm23751**	ScaRNA	SCARNA11
17	74	1.8	5.31E-09	**Gm23639**	SnoRNA	SNORA13
18	3334	1.8	1.18E-12	**Rny1**	Misc. RNA	RNY1
19	21	1.8	1.52E-05	**Gm23105**	SnoRNA	SNORA38
20	131	1.8	4.03E-11	**Gm23442**	SnoRNA	SNORA38
21	291	1.8	3.88E-11	**Snora7a**	SnoRNA	SNORA7a
22	30	1.7	2.60E-08	**Gm25777**	SnoRNA	SNORA77
23	32	1.7	1.61E-08	**Gm22786**	SnoRNA	SNORA26
24	39	1.7	1.96E-08	**Snord8**	SnoRNA	snord8
25	231	1.7	4.01E-08	**Gm25394**	SnoRNA	SNORA84
26	59	1.7	1.73E-08	**Hist1h2ad**	coding	NA
27	20	1.7	2.41E-06	**Gm16299**	antisense	NA
28	252	1.6	4.12E-06	**Snora24**	SnoRNA	SNORA24
29	1225	1.6	0.000149	**Gm24447**	misc RNA	NA
30	111	1.6	1.66E-08	**Gm22362**	SnoRNA	SNORA70
31	382	1.6	5.57E-08	**Snora78**	SnoRNA	SNORA78
32	4132	1.6	1.33E-09	**Rnu3a**	SnoRNA	NA
33	56	1.5	0.000162	**Gm38393**	coding	NA
34	35	1.5	1.09E-06	**Scarna9**	SnoRNA	Scarna9
35	104	1.5	4.43E-08	**Snora21**	SnoRNA	SNORA21

Figure 3. RNA-seq analysis of osteosarcoma tumors. (*A*) A plot smear of differentially expressed genes between p53 mutants versus p53-null tumors. (*B*) A heat map representing the differential expression of genes between p53 mutants versus p53-null. (*C*) Relative read counts of *p53* expression in *p53*-null and p53 mutant tumors. (*D*) List of the top 35 up-regulated genes in p53 mutant versus *p53*-null tumors. (*E*) Relative expression of the indicated snoRNAs in *p53*-null compared with p53 mutant tumors. (***) $P < 0.001$ by *t*-test.

orthologs of mouse snoRNAs. Twenty-one human orthologs were aligned (Fig. 3D), and ETS2 enrichment was found at nine of 21 identified SNORNA loci (Supplemental Fig. S7). Together, these analyses identified the Ets2 transcription factor as a strong candidate for the regulation of snoRNAs. Of note, mutant p53 is known to bind the Ets2 transcription factor and modulate its activity (Do et al. 2012).

To determine whether snoRNAs are regulated by mutant p53 via Ets2, we conditionally deleted *Ets2* in mutant p53 osteosarcomas by generating a cohort of *Osx-Cre;p53*$^{wm172/fl}$;*Ets2*$^{fl/fl}$ mice. Remarkably, homozygous deletion of *Ets2* yielded viable neonates with complete rescue of the malocclusion phenotype of *Osx-Cre* mice (Supplemental Fig. S8). This shows that Ets2 is functionally important in osteoblasts and bone development. These mice also developed osteosarcomas with complete penetrance, suggesting that loss of *Ets2* is not critical for tumor development. The survival of Osx-*Cre;p53*$^{wm172/fl}$;*Ets2*$^{fl/fl}$ mice overlapped with that of *Osx-Cre;p53*$^{fl/fl}$ mice (Fig. 4A). However, osteosarcomas derived from *Osx-Cre;p53*$^{wm172/fl}$;*Ets2*$^{fl/fl}$ mice showed a significant reduction in metastasis compared with *Osx-Cre;p53*$^{wm172/fl}$ mice ($P = 0.006$) (Fig. 4B). Of note, sagittal sections and fluorescent microscopy were used to identify micrometastasis as described for Figure 2M. These data suggest that the mutant p53 GOF phenotype can be modulated by *Ets2* deletion in vivo. More importantly, the metastatic phenotype of mutant p53 tumors is dampened once *Ets2* is deleted.

In order to evaluate the effect of *Ets2* loss on the mutant p53-driven transcriptome, we performed RNA-seq analysis on six tumors derived from *Osx-Cre;p53*$^{wm172/fl}$;*Ets2*$^{fl/fl}$ mice using the same platform and criteria used for samples derived from *Osx-Cre;p53*$^{wm172/fl}$ mice. On average, 65,954,162 reads were mapped for each osteosarcoma sample. Strikingly, the mutant p53-driven snoRNA signature (Fig. 3D) was strongly down-regulated in tumors derived from *Osx-Cre;p53*$^{wm172/fl}$;*Ets2*$^{fl/fl}$ mice as compared with those from *Osx-Cre;p53*$^{wm172/fl}$ mice (Fig. 4C). While not all 24 down-regulated snoRNAs had Ets2-binding motifs within 2 kb, all were down-regulated in the absence of *Ets2*. In addition to snoRNAs, we found that 88 of 179 (49%) genes up-regulated in *Osx-Cre;p53*$^{wm172/fl}$ tumors (as compared with *Osx-Cre;p53*$^{fl/fl}$) were down-regulated by deletion of Ets2. In addition, none of the 255 genes down-regulated in *Osx-Cre;p53*$^{wm172/fl}$ tumors versus *p53*$^{fl/fl}$ tumors was found down-regulated in *Ets2*-deleted tumors (Supplemental Fig. S9). These data indicate that mutant p53 regulation of approximately half of its target genes is mediated by the Ets2 transcription factor. Functional annotation of down-regulated genes in the absence of *Ets2* identified several pathways, including DNA methylation and histone modifications, to be highly down-regulated in *Ets2*-deleted tumors (Supplemental Fig. S10), suggesting that the mutant p53 GOF may be dependent in part on the Ets2 transcription factor.

Mutant and null p53 alleles involve distinct metastasis-associated gene networks

We further reanalyzed the RNA-seq data with a focus on the gene expression profile associated with metastasis, comparing four metastasizing versus four nonmetastasizing osteosarcomas in *p53* mutant mice. The same comparison was performed on four metastasizing versus four nonmetastasizing osteosarcomas with *p53*-null status. Surprisingly, we observed a small transcriptome difference between metastasizing and nonmetastasizing tumors in both p53 mutant and p53-null groups, suggesting that relatively few genes are critical to the acquisition of the metastatic capability. In p53 mutant tumors, 36 genes were identified to be significantly altered between metastasizing and nonmetastasizing groups (Fig. 5A). Strikingly, two members of glutamate receptors (*Grik2*

Table 1. *Distribution of the Ets2-binding motif at selected snoRNA loci*

Location	+/−	Bayesian branch length score	*Z*-score	FDR	Transcription factor	gene	Distance (base pairs)	Region
Chromosome 2: 86,215,610–86,215,617	−	2.3	3.81	0.026	ETS2	SNORD94	−886	Upstream
Chromosome X: 153,281,632–153,281,639	+	0.794	3.81	0.082	ETS2	SNORA70	−183	Upstream
Chromosome 17: 7,421,341–7,421,348	−	1.424	3.81	0.059	ETS2	SNORD1O	496	Downstream
Chromosome 5: 111,525,556–111,525,563	+	1.046	3.81	0.075	ETS2	SNORA13	476	Downstream
Chromosome 6: 31,697,945–31,697,952	+	0.965	3.81	0.077	ETS2	SNORA38	−889	Upstream
Chromosome 14: 80,739,176–80,739,183	−	1.427	3.81	0.059	ETS2	SNORA79	−252	Upstream
Chromosome 16: 57,144,124–57,144,131	+	1.197	3.81	0.069	ETS2	SNORA46	−4086	Upstream
Chromosome 11: 93,091,171–93,091,178	+	1.035	3.81	0.075	ETS2	SCARNA9	−3156	Upstream

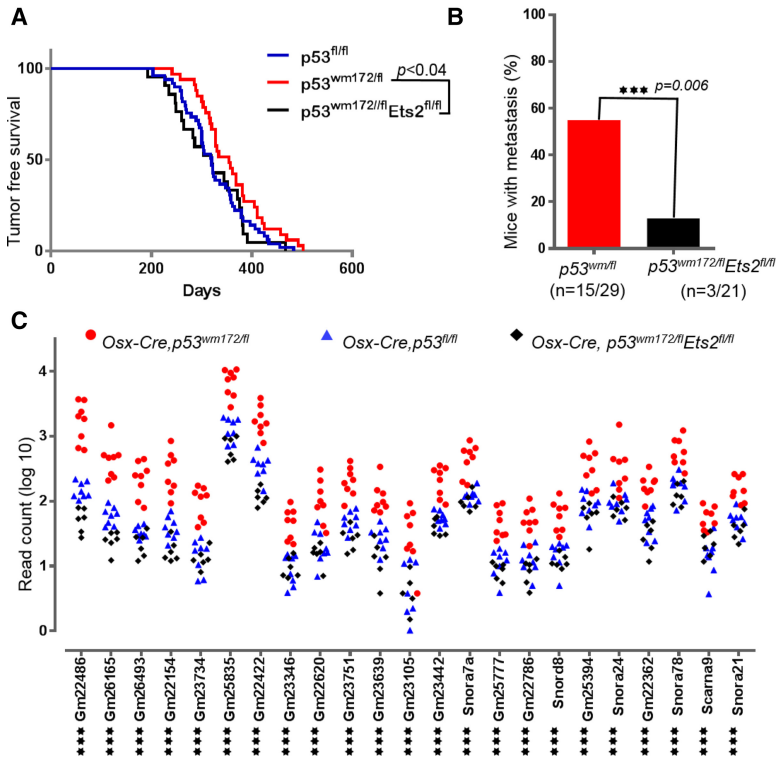

Figure 4. Characterization of conditional *Osx-Cre, p53*$^{wm172/fl}$;*Ets2*$^{fl/fl}$ mice. (*A*) Kaplan-Meier plot of tumor-free survival in conditional p53 mutant mice with loss of *Ets2*. (*B*) A bar chart representing the metastatic rate (percentage) of osteosarcomas developed in mice with the indicated genotypes. (*C*) Relative levels of snoRNA mRNAs ($\log_{10}$ transformed) in mice with the indicated genotypes. Significant differences between *Osx-Cre,p53*$^{wm172/fl}$;*Ets2*$^{fl/fl}$ and *Osx-Cre; p53*$^{wm172/fl}$ mice are indicated. (***) $P < 0.001$ by *t*-test.

and *Grin2c*) were on top of the list of genes that were significantly up-regulated in p53 mutant tumors with metastasis (Fig. 5A). Of note, glutamate receptor variants were found to contribute to osteosarcoma risk in a large human genome-wide association study (Savage et al. 2013). In *p53*-null tumors, we found 25 genes differentially expressed between metastasizing and nonmetastasizing tumors (Fig. 5B). None of these genes is known to be associated with metastasis. In addition, there was no overlap between data sets, suggesting that metastasis in p53 mutant tumors is transcriptionally distinct from *p53*-null tumors.

To further interrogate the metastasis phenotype of tumors in *p53* mutant and *p53*-null tumors, we performed whole-exome sequencing on the same samples used for RNA-seq. After sequencing, we first mapped sequencing reads to the mouse genome and then manually inspected all detected single-nucleotide variants (SNVs) in the IGV to make sure that mutation calls are not biased by poor read depth. We found that all four p53 mutant metastasizing osteosarcomas and none of the *p53*-null tumors harbored nonsynonymous mutations in *Ddias* (*DNA damage-induced apoptosis suppressor*), *Ticrr* (*TOPBP1-interacting checkpoint and replication regulator*), *Asph* (*aspartate* β*-hydroxylase*), *Nbn* (*Nibrin*), *Ggh* (γ*-glutamyl hydrolase*), and *Fanci* (*Fanconi anemia complementation group I*) genes. However the nonmetastasizing tumors did not have any mutations in those genes. In *p53*-null tumors, metastasis was found associated with mutations in *Mtus1* (*microtubule-associated tumor suppressor 1*) and *Clec1b* (*C-type lectin domain family 1 member B*). These data suggest that the metastasis-associated mutations are also distinct in p53 mutant tumors. To evaluate whether recurrent chromosomal aberrations might be associated with metastasis, we performed copy number analysis using these DNA sequencing data. We found that both p53 mutant and *p53*-null osteosarcomas displayed a considerable level of genome instability and copy number aberrations. However, we did not find any recurrent copy number changes associated with metastasis in either mutant p53 or *p53*-null tumors (Supplemental Fig. S11). Altogether, these results further support a distinct role of mutant p53 in driving metastasis.

Discussion

The most common *p53* alterations observed in human cancers are *p53* missense mutations that exhibit GOF phenotypes. Mice with *LSL-mutantp53* have been instrumental in studying mutant p53 GOF in vivo. However, the metastatic phenotype in these mice was confounded by the presence of p53 haploinsufficiency caused by the STOP cassette inserted into the *p53* locus. Here we describe a highly metastatic conditional somatic p53 mutant mouse model that closely mimics human osteosarcoma with complete penetrance. Moreover, we demonstrate that the prometastatic GOF phenotype of mutant p53 is regulated via the Ets2 transcription factor.

Previous studies have shown that loss of *p53* in osteoblasts can result in metastatic osteosarcoma (Berman et al. 2008; Walkley et al. 2008). In the present study, we generated a new mouse model harboring a single point mutation in *p53* in osteoblasts while preserving wild-

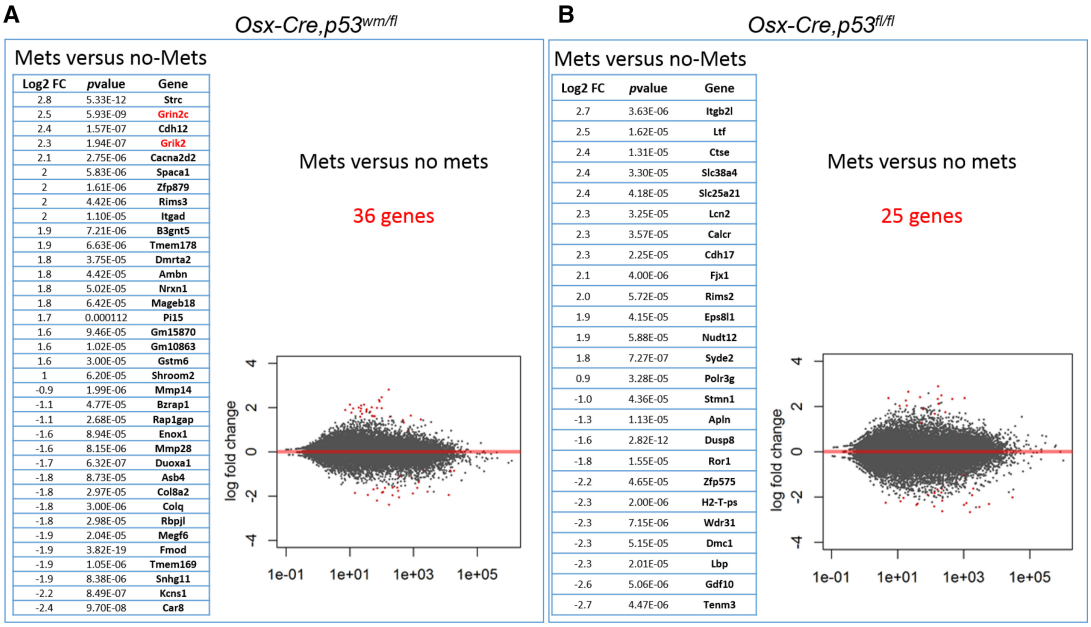

Figure 5. RNA-seq analysis in metastatic versus nonmetastatic tumors. (*A*) Differentially up-regulated genes are listed in the table. The plot smears represent the significant differentially expressed genes between metastasizing and nonmetastasizing in p53 mutant osteosarcomas. (*B*) The same representation as in *A* for mice with *p53*-null osteosarcomas.

type *p53* expression in all other tissues. This enabled us to evaluate the metastatic phenotype of the p53 mutant in a more physiologic model that more closely mimics sporadic osteosarcomas in humans. In our model, the p53 status of immune cells and stroma remains wild type, so there is no confounding effect of p53 haploinsufficiency in the cellular microenvironment that might affect tumor metastasis. Using a highly sensitive robust method for identifying microscopic metastases with fluorescent reporter genes, we demonstrated a significantly more aggressive prometastatic phenotype associated with the p53R172H point mutation in comparison with loss of p53.

Regulation of snoRNAs by mutant p53

While several studies have found evidence for the mutant p53 GOF phenotype in vivo (Lang et al. 2004; Olive et al. 2004; Berman et al. 2008), our work represents the first whole-transcriptome analysis of p53R172H mutant osteosarcomas and identifies a novel function of mutant p53 in the regulation of snoRNAs. Tumors with mutant p53 highly up-regulate a set of non-protein-coding snoRNA genes that have not been recognized previously as mutant p53 targets. snoRNAs regulate important cellular processes such as alternative splicing (Kishore and Stamm 2006), apoptosis in response to metabolic stress (Michel et al. 2011), and maintenance of open chromatin structure through an RNA–chromatin network (Schubert et al. 2012). Several snoRNAs have been identified to be significantly overexpressed in cancers such as non-small-cell lung cancer, acute leukemia, and metastatic prostate cancer (Martens-Uzunova et al. 2012; Valleron et al. 2012). However, the most intriguing role of snoRNA in metastatic cancer was identified recently by Liu et al. (2016). They found that tumor-derived exosomes contain snoRNAs that can activate TLR3, which consequently leads to chemokine secretion and neutrophil infiltration to establish a premetastatic niche. Unfortunately, a comprehensive human data set that includes snoRNA transcripts as well as p53 mutation status does not exist. Future work using shRNA knockdown of the snoRNA genes in syngeneic tumors should evaluate whether the snoRNA gene signature directly impacts metastasis in human cancer.

Mutant p53 GOF mediated by the Ets2 transcription factor

Mutations in the DNA-binding domain of p53 abolish binding to the p53 consensus sequence. However, previous studies show that mutant p53 can bind other transcription factors such as ETS2 through direct protein–protein interaction and drive its target genes (Do et al. 2012; Zhu et al. 2015). In this study, we found that at least a group of snoRNAs is highly up-regulated in p53 mutant tumors in an Ets2-dependent manner. Many of these snoRNAs harbor the Ets2-binding sites, although some do not. These may be regulated by downstream targets of Ets2. Deletion of *Ets2* in p53 mutant mice resulted in a strong down-regulation of these snoRNAs. More importantly, the metastatic phenotype observed in mutant p53 tumors was significantly inhibited after Ets2 depletion, further supporting the idea that the mutant p53 GOF phenotype is mediated in part by the Ets2 transcription factor. Our data do not examine a direct role for snoRNAs in metastasis, and the expression of these snoRNA genes may simply serve as a marker for mutant p53R172H

expression. Studies in a human prostate tumor cell line show that inhibition of Ets2 activity can strongly prevent invasion of a human prostate tumor cell line, providing additional data for the role of Ets2 in human cancer metastasis. (Foos and Hauser 2000). Taken together, our data strongly implicate Ets2 in the regulation of mutant p53 GOF and suggest a therapeutic potential for ETS2 inhibitors to inhibit metastasis driven by mutant p53R172H.

Materials and methods

Mice

Information on the construction of the p53 wmR172H targeting construct as well as the characterization of p53wmR172H mice (*p53*^{wm172}) has been described (Y Zhang, S Xiong, B Liu, V Pant, F Celii, G Chau, AC Elizondo-Fraire, P Yang, MJ You, AK El-Naggar, et al., in prep.). Transgenic Osx-Cre mice (*Sp7-tTA,tetO-EGFP/cre,* C57BL/6J*)* and mTmG transgenic mice (*ROSA*$^{mT/mG}$, 129/SvJ) were purchased from the Jackson laboratory. Mice bearing floxed alleles of the *p53* gene (*p53*^{fl}, C57BL/6J) have been described previously (Marino et al. 2000). Ets2 floxed mice (*Ets2*^{fl}, FVB/N) has been described (Wei et al. 2009). Animals were monitored every day for tumor formation and examined for malocclusion on a regular basis. Upon observation of visible masses, the tumor size was measured every few days. Tumors were processed for histology, and freshly frozen samples were kept at −80°C for genomic analysis. Animal studies were approved by the Institutional Animal Care and Use Committee (IACUC) at the University of Texas MD Anderson Cancer Center.

Tissue preparation and microscopy

Tissue preparation for hematoxylin and eosin (H&E) staining was performed as described previously (Jackson et al. 2012). The entire lungs were inflated with fixative and sectioned at 100 µm serially to detect micrometastatic lesions. For fluorescent microscopy, tissues were fixed overnight with 4% paraformaldehyde (PFA) in PBS (Sigma, P6148). Decalcification of bone as well as osteosarcoma tumors was performed in 14% EDTA solution under constant agitation for 3~5 d at 4 °C with refreshing 14% EDTA solution every 24 h. After decalcification, samples were washed with PBS for 2 h and soaked in 30% sucrose in PBS and 33% optimal cutting temperature (OCT) compound (Tissue-Tek, 4583) overnight at 4°C and then embedded in OCT. Embedded tissues were cut 5 µm thick using a cryostat. Slides were washed with PBS and soaked in 1 mM $MgCl_2$ in PBS for 30 min. The sections were then washed with PBS and mounted with VectaShield mounting medium (Vector Laboratories, H-1200). Images were captured on a fluorescence microscope (Eclipse 90i, Nikon) equipped with a Nikon DS-Fi1 color camera using Nikon Elements software. Some images were processed minimally in Adobe Photoshop only by histogram stretching and γ adjustment. To visualize GFP in the metastatic site, the organ was removed and placed in PBS in a six-well plate and imaged using an EVOS fluorescent microscope.

Quantitative PCR (qPCR)

RNA was isolated from cells using RNeasy kit (Qiagen, no. 74106) and was reverse-transcribed into cDNA using Maxima first strand cDNA synthesis kit (Frementas). The relative amount of gene transcripts was determined by real-time RT–PCR using SYBR Green master mix (Bio-Rad) and run on QuantStudio 6 Flex real-time PCR system (Applied Biosystems). The PCR protocol was carried out as recommended by Applied Biosystems. Standard curves for targets and housekeeping controls were based on the C_t (threshold cycle) values, and the relative concentrations of the standards and the relative concentrations for samples were calculated from the detected C_t values and the equation of the curves. Values obtained for targets were divided by the values of housekeeping genes (*Hprt*) to normalize for differences in reverse transcription. Genomic contamination of the samples was checked by "no amplification" control samples, which did not contain reverse transcriptase enzyme during the cDNA preparation.

RNA-seq

Barcoded Illumina-compatible stranded total RNA libraries were prepared using the TruSeq stranded total RNA sample preparation kit (Illumina). Briefly 250 ng of DNase I-treated total RNA was depleted of cytoplasmic and mitochondrial rRNA using Ribo-Zero Gold (Illumina). After purification, the RNA was fragmented using divalent cations, and double-stranded cDNA was synthesized using random primers. The ends of the resulting double-stranded cDNA fragments were repaired, 5′-phosphorylated, and 3′-A-tailed, and Illumina-specific indexed adapters were ligated. The products were purified and enriched with 12 cycles of PCR to create the final cDNA library. The libraries were quantified using the Qubit dsDNA HS assay kit, assessed for size distribution using Agilent Tapestation (Agilent Technologies), and then multiplexed eight libraries per pool. Library pools were quantified by qPCR and sequenced on the HiSeq 4000 sequencer using the 75-base-pair paired-end format. The raw RNA-seq readouts were subsequently mapped to the mouse mm10 assembly reference genome using TopHat2 and analyzed with DESeq2 (R/Bioconductor package) using and adjusted *P*-value of <0.05 as the significance cutoff. The pathway analysis was performed with Ingenuity Pathway Analysis (IPA; Ingenuity, Inc.).

Mouse exome sequencing

Illumina-compatible indexed libraries were prepared from 200 ng of Biorupter Ultrasonicator (Diagenode)-sheared guide DNA using the KAPA hyperlibrary preparation kit (Kapa Biosystems). The libraries were then prepared for capture with seven cycles of linker-mediated PCR (LM-PCR) amplification. Following LM-PCR, amplified libraries were assessed for quality using the TapeStation high-sensitivity DNA kit (Agilent Technologies) and for quantity using the Qubit dsDNA HS assay kit (ThermoFisher) and then multiplexed eight libraries per pool for exome capture. Exome capture was performed using the NimbleGen SeqCap EZ developer kit. Following capture, the enriched libraries were amplified with seven cycles of PCR. Amplified libraries were assessed for exon target enrichment by qPCR, assessed for the size distribution using the Agilent TapesStation, and quantified using the Qubit dsDNA HS assay kit. Sequencing was performed on a HiSeq 4000 sequencer (Illumina, Inc.), loading 16 samples (two captures) per lane and sequencing using the 76-nt paired-end configuration. The raw sequencing reads were mapped to the mouse genome reference (GRCm38/mm10) with a BWA alignment tool. The aligned data were processed and analyzed using GATK tools (Broad Institute). Somatic mutation annotations were performed with the ANNOVAR tool. The mouse snp138 was used to filter the mouse single-nucleotide polymorphisms (SNPs).

Copy number calculation from WES data

Copy numbers were calculated from the aligned BAM files using the cnMOPS package (Klambauer et al. 2012). First, the total

number of mapped reads was summarized by the mouse exon capture target regions, and then the integer copy numbers were calculated and followed by segmentation using the "calcIntegerCopyNumbers" and "segmentation" functions in the cnMOPS package (Klambauer et al. 2012). To construct the clustering heat maps, the integer copy numbers were transformed into $[\log_2 (\text{ratio} + 0.1)]$, and the Euclidean distances were calculated from the transformed data matrix, where each column represents one sample, and each row contains the $[\log_2 (\text{ratio} + 0.1)]$ transformed data of each segment. The one-dimensional hierarchical clustering was performed in R using the heatmap3 function available on CRAN (https://www.r-project.org) with the "ward.D2" linkage, and the *X*-axis was ordered by mouse genome positions.

FACS analysis and cell sorting

Single-cell suspensions from bone and osteosarcoma tumor samples were collected and processed in the Flow Cytometry and Cellular Imaging Core Facilities at the University of Texas MD Anderson Cancer Center on a FACS Calibur flow cytometer, and analysis was performed with FlowJo software. Sorted cells were kept at −80°C until use.

Statistical analysis

Means, standard deviation, and 95% confidence intervals were calculated. Student's *t*-test was used for comparative analysis.

Acknowledgments

We sincerely thank Nikita and Chris in the Animal Facility, Wendy Schober and her team in the Flow Cytometry Core, Keith Michel in the Imaging Facility, Hongli Tang in the Sequencing Facility, Asha Multani in the Cytogenetic Facility, and Adriana Paulucci-Holthauzen in the Microscopy Laboratory. Thanks are also due to Anthon Berns for providing $p53^{fl}$ mice. This work was funded by a Cancer Prevention Research Institute of Texas (CPRIT) grant (RP160250) and a National Institutes of Health grant (CA82577) to G.L., and Cancer Center Support Grant CA016672.

References

Berman SD, Calo E, Landman AS, Danielian PS, Miller ES, West JC, Fonhoue BD, Caron A, Bronson R, Bouxsein ML, et al. 2008. Metastatic osteosarcoma induced by inactivation of Rb and p53 in the osteoblast lineage. *Proc Natl Acad Sci* **105:** 11851–11856.

Bielack SS, Kempf-Bielack B, Delling G, Exner GU, Flege S, Helmke K, Kotz R, Salzer-Kuntschik M, Werner M, Winkelmann W, et al. 2002. Prognostic factors in high-grade osteosarcoma of the extremities or trunk: an analysis of 1,702 patients treated on neoadjuvant cooperative osteosarcoma study group protocols. *J Clin Oncol* **20:** 776–790.

Chaffer CL, Weinberg RA. 2011. A perspective on cancer cell metastasis. *Science* **331:** 1559–1564.

Djebali S, Davis CA, Merkel A, Dobin A, Lassmann T, Mortazavi A, Tanzer A, Lagarde J, Lin W, Schlesinger F, et al. 2012. Landscape of transcription in human cells. *Nature* **489:** 101–108.

Do PM, Varanasi L, Fan S, Li C, Kubacka I, Newman V, Chauhan K, Daniels SR, Boccetta M, Garrett MR, et al. 2012. Mutant p53 cooperates with ETS2 to promote etoposide resistance. *Genes Dev* **26:** 830–845.

Doyle B, Morton JP, Delaney DW, Ridgway RA, Wilkins JA, Sansom OJ. 2010. p53 mutation and loss have different effects on tumourigenesis in a novel mouse model of pleomorphic rhabdomyosarcoma. *J Pathol* **222:** 129–137.

Fabbri M, Paone A, Calore F, Galli R, Gaudio E, Santhanam R, Lovat F, Fadda P, Mao C, Nuovo GJ, et al. 2012. MicroRNAs bind to Toll-like receptors to induce prometastatic inflammatory response. *Proc Natl Acad Sci* **109:** E2110–E2116.

Foos G, Hauser CA. 2000. Altered Ets transcription factor activity in prostate tumor cells inhibits anchorage-independent growth, survival, and invasiveness. *Oncogene* **19:** 5507–5516.

Freed-Pastor WA, Mizuno H, Zhao X, Langerod A, Moon SH, Rodriguez-Barrueco R, Barsotti A, Chicas A, Li W, Polotskaia A, et al. 2012. Mutant p53 disrupts mammary tissue architecture via the mevalonate pathway. *Cell* **148:** 244–258.

Jackson JG, Pant V, Li Q, Chang LL, Quintas-Cardama A, Garza D, Tavana O, Yang P, Manshouri T, Li Y, et al. 2012. p53-mediated senescence impairs the apoptotic response to chemotherapy and clinical outcome in breast cancer. *Cancer Cell* **21:** 793–806.

Jonkers J, Meuwissen R, van der Gulden H, Peterse H, van der Valk M, Berns A. 2001. Synergistic tumor suppressor activity of BRCA2 and p53 in a conditional mouse model for breast cancer. *Nat Genet* **29:** 418–425.

Kalo E, Kogan-Sakin I, Solomon H, Bar-Nathan E, Shay M, Shetzer Y, Dekel E, Goldfinger N, Buganim Y, Stambolsky P, et al. 2012. Mutant p53R273H attenuates the expression of phase 2 detoxifying enzymes and promotes the survival of cells with high levels of reactive oxygen species. *J Cell Sci* **125:** 5578–5586.

Kim MP, Lozano G. 2017. Mutant p53 partners in crime. *Cell Death Differ* (in press).

Kishore S, Stamm S. 2006. The snoRNA HBII-52 regulates alternative splicing of the serotonin receptor 2C. *Science* **311:** 230–232.

Kiss-Laszlo Z, Henry Y, Bachellerie JP, Caizergues-Ferrer M, Kiss T. 1996. Site-specific ribose methylation of preribosomal RNA: a novel function for small nucleolar RNAs. *Cell* **85:** 1077–1088.

Klambauer G, Schwarzbauer K, Mayr A, Clevert DA, Mitterecker A, Bodenhofer U, Hochreiter S. 2012. cn.MOPS: mixture of Poissons for discovering copy number variations in next-generation sequencing data with a low false discovery rate. *Nucleic Acids Res* **40:** e69.

Lang GA, Iwakuma T, Suh YA, Liu G, Rao VA, Parant JM, Valentin-Vega YA, Terzian T, Caldwell LC, Strong LC, et al. 2004. Gain of function of a p53 hot spot mutation in a mouse model of Li-Fraumeni syndrome. *Cell* **119:** 861–872.

Lengner CJ, Steinman HA, Gagnon J, Smith TW, Henderson JE, Kream BE, Stein GS, Lian JB, Jones SN. 2006. Osteoblast differentiation and skeletal development are regulated by Mdm2-p53 signaling. *J Cell Biol* **172:** 909–921.

Leroy B, Fournier JL, Ishioka C, Monti P, Inga A, Fronza G, Soussi T. 2013. The TP53 Website: an integrative resource centre for the TP53 mutation database and TP53 mutant analysis. *Nucleic Acids Res* **41:** D962–D969.

Liu Y, Gu Y, Han Y, Zhang Q, Jiang Z, Zhang X, Huang B, Xu X, Zheng J, Cao X. 2016. Tumor exosomal RNAs promote lung pre-metastatic niche formation by activating alveolar epithelial TLR3 to recruit neutrophils. *Cancer Cell* **30:** 243–256.

Makarova JA, Kramerov DA. 2011. SNOntology: myriads of novel snoRNAs or just a mirage? *BMC Genomics* **12:** 543.

Marino S, Vooijs M, van Der Gulden H, Jonkers J, Berns A. 2000. Induction of medulloblastomas in p53-null mutant mice by

somatic inactivation of Rb in the external granular layer cells of the cerebellum. *Genes Dev* **14:** 994–1004.

Martens-Uzunova ES, Jalava SE, Dits NF, van Leenders GJ, Moller S, Trapman J, Bangma CH, Litman T, Visakorpi T, Jenster G. 2012. Diagnostic and prognostic signatures from the small non-coding RNA transcriptome in prostate cancer. *Oncogene* **31:** 978–991.

Mehlen P, Puisieux A. 2006. Metastasis: a question of life or death. *Nat Rev Cancer* **6:** 449–458.

Michel CI, Holley CL, Scruggs BS, Sidhu R, Brookheart RT, Listenberger LL, Behlke MA, Ory DS, Schaffer JE. 2011. Small nucleolar RNAs U32a, U33, and U35a are critical mediators of metabolic stress. *Cell Metab* **14:** 33–44.

Mizoguchi T, Pinho S, Ahmed J, Kunisaki Y, Hanoun M, Mendelson A, Ono N, Kronenberg HM, Frenette PS. 2014. Osterix marks distinct waves of primitive and definitive stromal progenitors during bone marrow development. *Dev Cell* **29:** 340–349.

Morton JP, Timpson P, Karim SA, Ridgway RA, Athineos D, Doyle B, Jamieson NB, Oien KA, Lowy AM, Brunton VG, et al. 2010. Mutant p53 drives metastasis and overcomes growth arrest/senescence in pancreatic cancer. *Proc Natl Acad Sci* **107:** 246–251.

Muller PA, Vousden KH. 2014. Mutant p53 in cancer: new functions and therapeutic opportunities. *Cancer Cell* **25:** 304–317.

Muller PA, Caswell PT, Doyle B, Iwanicki MP, Tan EH, Karim S, Lukashchuk N, Gillespie DA, Ludwig RL, Gosselin P, et al. 2009. Mutant p53 drives invasion by promoting integrin recycling. *Cell* **139:** 1327–1341.

Olive KP, Tuveson DA, Ruhe ZC, Yin B, Willis NA, Bronson RT, Crowley D, Jacks T. 2004. Mutant p53 gain of function in two mouse models of Li-Fraumeni syndrome. *Cell* **119:** 847–860.

Olivier M, Hollstein M, Hainaut P. 2010. TP53 mutations in human cancers: origins, consequences, and clinical use. *Cold Spring Harb Perspect Biol* **2:** a001008.

Oren M, Rotter V. 2010. Mutant p53 gain-of-function in cancer. *Cold Spring Harb Perspect Biol* **2:** a001107.

Patocs A, Zhang L, Xu Y, Weber F, Caldes T, Mutter GL, Platzer P, Eng C. 2007. Breast-cancer stromal cells with TP53 mutations and nodal metastases. *N Engl J Med* **357:** 2543–2551.

Pfister NT, Fomin V, Regunath K, Zhou JY, Zhou W, Silwal-Pandit L, Freed-Pastor WA, Laptenko O, Neo SP, Bargonetti J, et al. 2015. Mutant p53 cooperates with the SWI/SNF chromatin remodeling complex to regulate VEGFR2 in breast cancer cells. *Genes Dev* **29:** 1298–1315.

Rodda SJ, McMahon AP. 2006. Distinct roles for Hedgehog and canonical Wnt signaling in specification, differentiation and maintenance of osteoblast progenitors. *Development* **133:** 3231–3244.

Savage SA, Mirabello L, Wang Z, Gastier-Foster JM, Gorlick R, Khanna C, Flanagan AM, Tirabosco R, Andrulis IL, Wunder JS, et al. 2013. Genome-wide association study identifies two susceptibility loci for osteosarcoma. *Nat Genet* **45:** 799–803.

Schubert T, Pusch MC, Diermeier S, Benes V, Kremmer E, Imhof A, Langst G. 2012. Df31 protein and snoRNAs maintain accessible higher-order structures of chromatin. *Mol Cell* **48:** 434–444.

Tycowski KT, Shu MD, Steitz JA. 1996. A mammalian gene with introns instead of exons generating stable RNA products. *Nature* **379:** 464–466.

Valleron W, Laprevotte E, Gautier EF, Quelen C, Demur C, Delabesse E, Agirre X, Prosper F, Kiss T, Brousset P. 2012. Specific small nucleolar RNA expression profiles in acute leukemia. *Leukemia* **26:** 2052–2060.

Walkley CR, Qudsi R, Sankaran VG, Perry JA, Gostissa M, Roth SI, Rodda SJ, Snay E, Dunning P, Fahey FH, et al. 2008. Conditional mouse osteosarcoma, dependent on p53 loss and potentiated by loss of Rb, mimics the human disease. *Genes Dev* **22:** 1662–1676.

Wei G, Srinivasan R, Cantemir-Stone CZ, Sharma SM, Santhanam R, Weinstein M, Muthusamy N, Man AK, Oshima RG, Leone G, et al. 2009. Ets1 and Ets2 are required for endothelial cell survival during embryonic angiogenesis. *Blood* **114:** 1123–1130.

Williams GT, Farzaneh F. 2012. Are snoRNAs and snoRNA host genes new players in cancer? *Nat Rev Cancer* **12:** 84–88.

Xie X, Rigor P, Baldi P. 2009. MotifMap: a human genome-wide map of candidate regulatory motif sites. *Bioinformatics* **25:** 167–174.

Xiong S, Tu H, Kollareddy M, Pant V, Li Q, Zhang Y, Jackson JG, Suh YA, Elizondo-Fraire AC, Yang P, et al. 2014. Pla2g16 phospholipase mediates gain-of-function activities of mutant p53. *Proc Natl Acad Sci* **111:** 11145–11150.

Zhu J, Sammons MA, Donahue G, Dou Z, Vedadi M, Getlik M, Barsyte-Lovejoy D, Al-awar R, Katona BW, Shilatifard A, et al. 2015. Gain-of-function p53 mutants co-opt chromatin pathways to drive cancer growth. *Nature* **525:** 206–211.